Thermodynamic Properties of Phosphorus Oxide in the $2CaO{\cdot}SiO_2$-$3CaO{\cdot}P_2O_5$ Solid Solution Saturated with MgO

MING ZHONG, HIROYUKI MATSUURA, and FUMITAKA TSUKIHASHI

Molten iron was equilibrated with various compositions of the $2CaO{\cdot}SiO_2$-$3CaO{\cdot}P_2O_5$ solid solution saturated with MgO with the oxygen partial pressure of 5.22×10^{-12} atm at 1823 K (1550 °C) and 1.41×10^{-11} atm at 1873 K (1600 °C). From the concentration of P in molten iron at equilibrium, the activity of P_2O_5 relative to the hypothetical pure liquid P_2O_5 was determined. The saturating MgO phase at equilibrium was detected by X-ray diffraction for each sample, and thus, the activity of $3MgO{\cdot}P_2O_5$ was also estimated. The activity of P_2O_5 and $3MgO{\cdot}P_2O_5$ increased with the increase of $3CaO{\cdot}P_2O_5$ content in the solid solution. In addition, the activity of P_2O_5 in the $2CaO{\cdot}SiO_2$-$3CaO{\cdot}P_2O_5$ solid solution saturated with MgO was larger than that saturated with CaO.

DOI: 10.1007/s11663-016-0639-4

I. INTRODUCTION

SINCE phosphorus segregates in the grain boundary of austenite, which increases the fracture appearance transition temperature to cause the cold embrittlement of steel,[1] it should be removed from molten iron and steel during the dephosphorization process as much as possible. Usually CaO is adopted for the dephosphorization process, and in most cases, extra CaO is added to slag to achieve a high dephosphorization efficiency, while the CaO consumption and slag volume significantly increase. Meanwhile, the generated slag after the dephosphorization process is hard to be recycled since the unreacted CaO remains in slag or CaO-based compounds precipitate during the solidification of slag.

It is well known that CaO reacts with SiO_2 to form $2CaO{\cdot}SiO_2$ on the surface of CaO in the CaO-FeO-SiO_2-P_2O_5 system during the dephosphorization process and then $2CaO{\cdot}SiO_2$ reacts with P_2O_5 to form the $2CaO{\cdot}SiO_2$-$3CaO{\cdot}P_2O_5$ solid solution.[2–4] In addition, $2CaO{\cdot}SiO_2$ and $3CaO{\cdot}P_2O_5$ form a pseudo-binary solid solution over a wide composition range at steelmaking temperature.[5] Based on the large partition ratio of P_2O_5 between the solid solution and liquid slag,[6–8] the multiphase flux has been considered for use in the dephosphorization process.

To understand the multiphase flux better, the reaction mechanisms between solid CaO or $2CaO{\cdot}SiO_2$ and the FeO_x-CaO-SiO_2-P_2O_5 system have been intensively studied.[9–15] The phase relationship for the CaO-FeO-SiO_2-P_2O_5($-Al_2O_3$) system has been also studied.[16–18] The activity of P_2O_5 in the $2CaO{\cdot}SiO_2$-$3CaO{\cdot}P_2O_5$ solid solution has been measured by the chemical equilibration method at 1573 K (1300 °C) by Hasegawa *et al.*[19] or at 1823 and 1873 K (1550 and 1600 °C) by the current authors.[20] Since the excess CaO is being added to slag in the actual dephosphorization process, the thermodynamics of the $2CaO{\cdot}SiO_2$-$3CaO{\cdot}P_2O_5$ solid solution saturated with CaO has been also investigated by the current authors.[21] In the current study, the thermodynamic properties of the $2CaO{\cdot}SiO_2$-$3CaO{\cdot}P_2O_5$ solid solution saturated with MgO were measured to investigate the effect of MgO on the property of P_2O_5 in the $2CaO{\cdot}SiO_2$-$3CaO{\cdot}P_2O_5$ solid solution since the dephosphorization slag contains a certain amount of MgO.

II. EXPERIMENTAL

The $2CaO{\cdot}SiO_2$-$3CaO{\cdot}P_2O_5$ solid solution saturated with MgO was equilibrated with molten iron at 1823 and 1873 K (1550 and 1600 °C). The mixture of SiO_2, $CaHPO_4{\cdot}2H_2O$, MgO, and CaO was sintered to prepare the $2CaO{\cdot}SiO_2$-$3CaO{\cdot}P_2O_5$ solid solution powder containing MgO or both MgO and CaO. The mixture was heated in air at 1873 K (1600 °C) in a platinum crucible for 48 hours, and then the sintered material was ground into fine powder before sintering for the next 48 hours. After the second sintering, the mixture was ground into fine powder again and about 1.5 g powder was charged in steel dies to be pressed into a cylindrical specimen (diameter: 18 mm, thickness: 3 mm) at 50 MPa. The initial compositions of oxide specimens are summarized in Table I and shown on the CaO-SiO_2-P_2O_5 ternary diagram in Figure 1.

MING ZHONG, formerly Ph.D. Student with the Department of Advanced Materials Science, Graduate School of Frontier Sciences, The University of Tokyo, 5-1-5 Kashiwanoha, Kashiwa, Chiba 277-8561, Japan, is now Researcher with the Institute of Advanced Energy, Kyoto University, Gokasho, Uji, Kyoto 611-0011, Japan. H. MATSUURA, Associate Professor, and F. TSUKIHASHI, Professor, are with the Department of Advanced Materials Science, Graduate School of Frontier Sciences, The University of Tokyo. Contact e-mail: matsuura@k.u-tokyo.ac.jp

Manuscript submitted November 13, 2015.
Article published online March 14, 2016.

Table I. Initial Composition of Oxide Specimen and Equilibrium Temperature

No.	T/K (T/°C)	Composition of Oxide Specimen/Mass Percent							
		CaO	SiO_2	P_2O_5	MgO	$2CaO{\cdot}SiO_2$	$3CaO{\cdot}P_2O_5$	MgO	CaO
1-1	1823 (1550)	47.8	21.2	7.0	24.0	60.8	15.2	24.0	0.0
1-2	1823 (1550)	46.2	15.9	13.9	24.0	45.6	30.4	24.0	0.0
1-3	1823 (1550)	44.5	10.6	20.9	24.0	30.4	45.6	24.0	0.0
1-4	1823 (1550)	42.9	5.3	27.8	24.0	15.2	60.8	24.0	0.0
2-1	1873 (1600)	47.8	21.2	7.0	24.0	60.8	15.2	24.0	0.0
2-2	1873 (1600)	46.2	15.9	13.9	24.0	45.6	30.4	24.0	0.0
2-3	1873 (1600)	44.5	10.6	20.9	24.0	30.4	45.6	24.0	0.0
2-4	1873 (1600)	42.9	5.3	27.8	24.0	15.2	60.8	24.0	0.0
3-1	1823 (1550)	57.9	25.7	8.4	8.0	73.6	18.4	8.0	0.0
3-2	1823 (1550)	55.9	19.2	16.9	8.0	55.2	36.8	8.0	0.0
3-3	1823 (1550)	53.9	12.8	25.3	8.0	36.8	55.2	8.0	0.0
3-4	1823 (1550)	51.9	6.4	33.7	8.0	18.4	73.6	8.0	0.0
4-1	1873 (1600)	57.9	25.7	8.4	8.0	73.6	18.4	8.0	0.0
4-2	1873 (1600)	55.9	19.2	16.9	8.0	55.2	36.8	8.0	0.0
4-3	1873 (1600)	53.9	12.8	25.3	8.0	36.8	55.2	8.0	0.0
4-4	1873 (1600)	51.9	6.4	33.7	8.0	18.4	73.6	8.0	0.0
5-1	1823 (1550)	55.6	10.9	9.5	24.0	31.2	20.8	24.0	24.0
5-2	1873 (1600)	55.6	10.9	9.5	24.0	31.2	20.8	24.0	24.0

Since the phase relationship of the CaO-SiO_2-P_2O_5 system at 1823 and 1873 K (1550 and 1600 °C) is deficient, the boundary and tie lines in Figure 1 were determined at 1773 K (1500 °C) after Gutt.[22] The formation of desired phases was confirmed by X-ray diffraction (XRD). In all oxide specimens, the MgO phase was detected and the CaO phase was also detected in oxide specimens of Nos. 5-1 and 5-2. The XRD patterns of oxide specimens Nos. 1-2 and 5-1 are shown as examples in Figures 2 and 3, respectively.

For achieving the equilibrium quickly, only 10 g of electrolytic iron with the initial concentration of P < 0.0003 mass pct was equilibrated with the prepared cylindrical oxide in a magnesia crucible (outer diameter: 25 mm, inner diameter: 20 mm, height: 60 mm) in an alumina reaction tube (outer diameter: 60 mm, inner diameter: 50 mm, length: 1000 mm). The equilibrium duration was 24 hours, which was enough to reach the equilibrium confirmed by previous research.[20,21] Temperature of the hot zone was determined by a B-type thermocouple before each experiment, and the experimental temperature was monitored by a B-type thermocouple placed at the bottom of the magnesia crucible. The oxygen partial pressure was controlled by the mixture of CO and CO_2 gases with the total flow rate of 366 mL/min according to Eq. [1]. The oxygen partial pressure was 5.22×10^{-12} atm at 1823 K (1550 °C) or 1.41×10^{-11} atm at 1873 K (1600 °C) with the CO/CO_2 ratio of 110/1:

$$CO(g) + 1/2O_2(g) = CO_2(g),$$

$$\Delta G_1^\circ = -281000 + 85.23T \text{ J/mol}^{[23]}. \quad [1]$$

After the equilibrium was established, the sample was quenched by Ar stream at the outside of the furnace. Concentrations of P in iron and P_2O_5 in oxide specimen were analyzed by spectrophotometry. Compositions of CaO, FeO, and MgO in oxide specimen were determined by ICP-OES and that of SiO_2 was determined by gravimetry.

III. RESULTS AND DISCUSSION

Oxide specimens of Nos. 2-4 and 4-4 turned into molten slag after experiments as shown by open circles in Figure 1. The concentration of P in iron and the composition of oxide specimen after reaction are summarized in Table II and shown on the CaO-SiO_2-P_2O_5 ternary diagram in Figure 4.

Since molten iron coexisted, iron oxide in the oxide specimen was assumed to be FeO. At equilibrium, the MgO phase was detected in all oxide specimen and the CaO phase was also detected in the oxide specimen of Nos. 5-1 and 5-2 by XRD. The mole fraction of $3CaO{\cdot}P_2O_5$ in the $2CaO{\cdot}SiO_2$-$3CaO{\cdot}P_2O_5$ solid solution shown in Table III was calculated from the analyzed compositions of SiO_2 and P_2O_5 by assuming the pure pseudo-binary solid solution.

A. *Equilibrium Concentration of P in Molten Iron and the Phosphorus Partition Ratio Between Solid Mixture and Molten Iron*

The equilibrium concentration of P in molten iron and the phosphorus partition ratio between the mixture of the $2CaO{\cdot}SiO_2$-$3CaO{\cdot}P_2O_5$ solid solution and MgO and molten iron are shown in Figures 5 and 6 as a function of $3CaO{\cdot}P_2O_5$ content in the solid solution, respectively. The concentration of P in molten iron increased with the increase of the $3CaO{\cdot}P_2O_5$ content in the solid solution. By comparing at the same composition of the solid solution, the concentration of P at

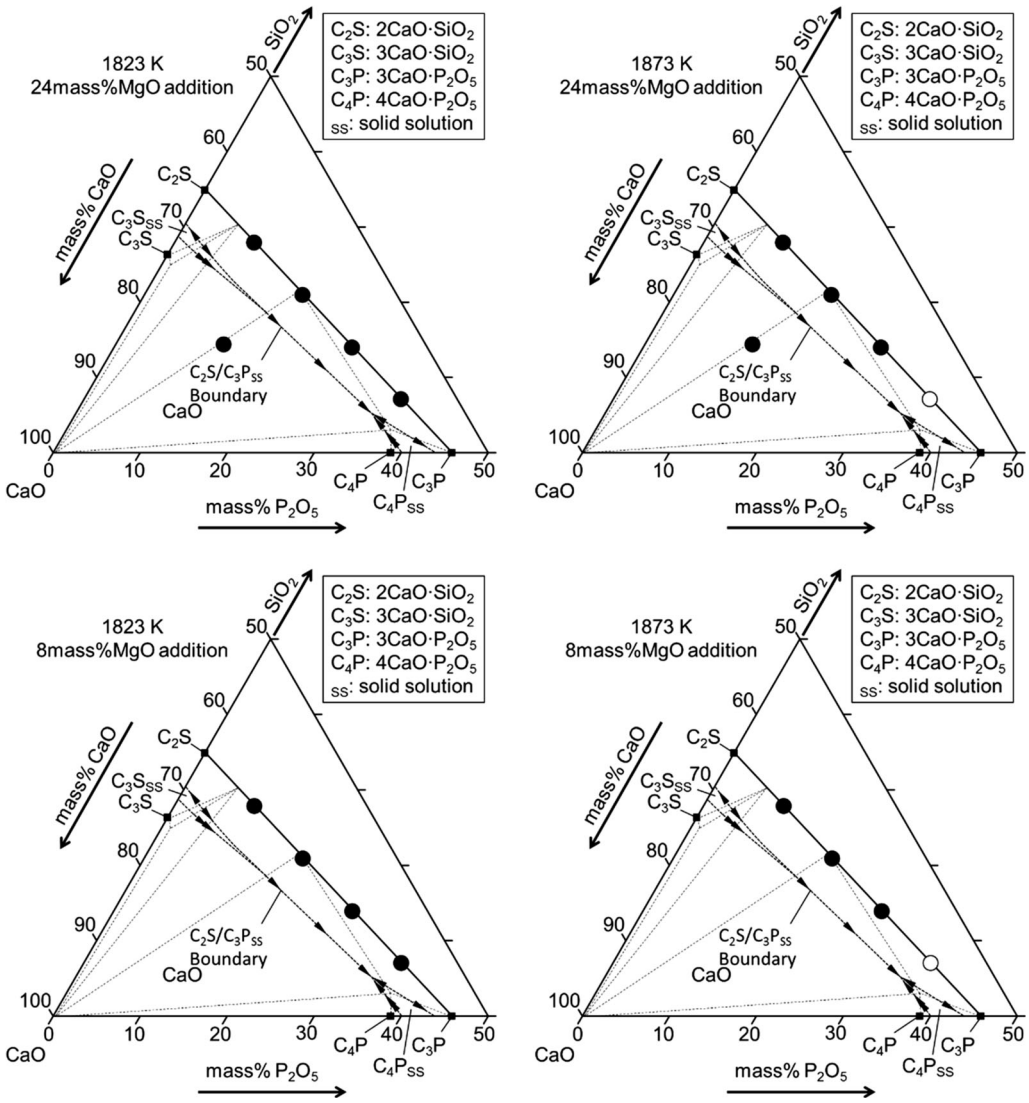

Fig. 1—Projection of the initial composition of oxide specimen onto the $CaO-SiO_2-P_2O_5$ ternary system. The specimens marked as open circles turned into molten slag at equilibrium. The boundary and tie lines in the phase diagram were determined at 1773 K (1500 °C) by Gutt.[22]

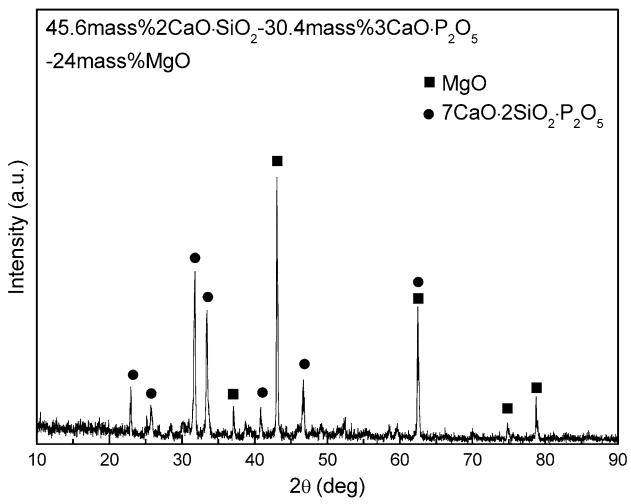

Fig. 2—XRD pattern of the oxide specimen containing 45.6 mass pct $2CaO·SiO_2$, 30.4 mass pct $3CaO·P_2O_5$, and 24 mass pct MgO.

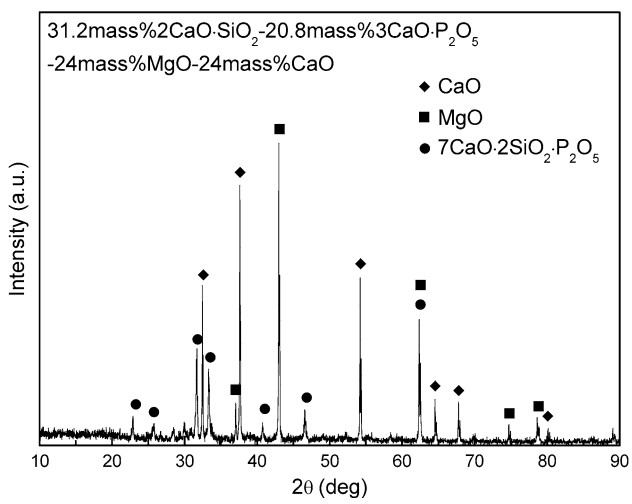

Fig. 3—XRD pattern of the oxide specimen containing 31.2 mass pct $2CaO·SiO_2$, 20.8 mass pct $3CaO·P_2O_5$, 24 mass pct MgO, and 24 mass pct CaO.

Table II. Composition of Oxide Specimen and the Concentration of P in Iron at Equilibrium

No.	Composition of Oxide Specimen/Mass Percent						P in Iron/Mass Percent
	P_2O_5	SiO_2	CaO	MgO	FeO	Total	
1-1	7.0	19.7	46.0	23.4	0.607	96.7	0.00506
1-2	13.8	16.0	44.4	23.1	0.643	97.9	0.0124
1-3	21.1	10.7	42.7	23.7	0.645	98.8	0.0179
1-4	27.9	5.3	41.5	23.0	0.451	98.2	0.0292
2-1	6.9	21.0	45.6	23.2	0.857	97.6	0.00798
2-2	13.8	16.3	44.2	23.5	1.32	99.1	0.0171
2-3	21.0	10.6	42.7	23.7	1.29	99.3	0.0220
3-1	8.5	24.8	55.9	7.5	0.482	97.2	0.00635
3-2	16.8	18.6	54.0	7.8	0.499	97.7	0.00903
3-3	24.3	12.4	52.5	7.9	0.478	97.6	0.0206
3-4	33.7	6.32	50.9	7.8	0.339	99.1	0.0372
4-1	8.3	24.1	55.7	8.4	0.768	97.3	0.00995
4-2	16.5	18.2	52.8	8.7	0.538	96.7	0.0213
4-3	24.0	12.6	52.4	8.5	0.427	97.9	0.0369
5-1	9.3	10.0	52.9	23.0	0.760	96.0	0.00603
5-2	9.2	10.0	51.7	23.5	1.25	95.7	0.0142

1873 K (1600 °C) was larger than that at 1823 K (1550 °C). The phosphorus partition ratio did not change with the $3CaO{\cdot}P_2O_5$ content in the solid solution significantly. The effect of MgO content on the phosphorus partition ratio was also not obvious.

B. *FeO Content and Activity Coefficient of FeO in the $2CaO{\cdot}SiO_2$-$3CaO{\cdot}P_2O_5$ Solid Solution Saturated with MgO*

The FeO content in the oxide specimen at equilibrium is shown in Figure 7 as a function of P_2O_5 content. For most samples, the content of FeO was <1 mass pct. According to Eq. [2], the activity of FeO relative to hypothetical pure liquid FeO was calculated to be 7.75×10^{-2} at 1823 K (1550 °C) with the oxygen partial pressure of 5.22×10^{-12} atm, or 8.15×10^{-2} at 1873 K (1600 °C) with the oxygen partial pressure of 1.41×10^{-11} atm:

$$\mathrm{FeO(l)} = \mathrm{Fe(l)} + 1/2\mathrm{O_2(g)},$$

$$\Delta G_2^\circ = 256000 - 53.68T \ \mathrm{J/mol}^{[23]}. \qquad [2]$$

The activity coefficient of FeO is shown in Figure 8 and Table III as a function of the $3CaO{\cdot}P_2O_5$ content in the solid solution. The activity coefficient of FeO at 1873 K (1600 °C) was larger than that at 1823 K (1550 °C). Significant influence of CaO or MgO addition on the activity coefficient of FeO was not observed.

C. *Activity and Activity Coefficient of P_2O_5 in the $2CaO{\cdot}SiO_2$-$3CaO{\cdot}P_2O_5$ Solid Solution Saturated with MgO*

Due to the inevitable segregation during quenching, the concentrations of C and O in molten iron were calculated by Eqs. [3] and [4] and the reported interaction coefficients shown in Table IV instead of the analyzed values.

The analytical concentration of P in iron was not significantly affected by the segregation since the segregated P remained in the iron sample after quenching:

$$\underline{\mathrm{O}}(\text{mass pct}) + \mathrm{CO(g)} = \mathrm{CO_2(g)},$$

$$\Delta G_3^\circ = -166900 + 91.16T \ \mathrm{J/mol}^{[24]}, \qquad [3]$$

$$\underline{\mathrm{C}}(\text{mass pct}) + \mathrm{CO_2(g)} = 2\mathrm{CO(g)},$$

$$\Delta G_4^\circ = -144700 + 129.5T \ \mathrm{J/mol}^{[24]}, \qquad [4]$$

$$\mathrm{P_2O_5(l)} = 2\underline{\mathrm{P}}(\text{mass pct}) + 5\underline{\mathrm{O}}(\text{mass pct}),$$

$$\Delta G_5^\circ = -832384 - 632.65T \ \mathrm{J/mol}^{[25]}. \qquad [5]$$

The activity of P_2O_5 relative to the hypothetical liquid P_2O_5 was calculated by Eq. [5] from the concentration of P in molten iron and the reported thermodynamic data.[25] The activity and activity coefficient of P_2O_5 in the $2CaO{\cdot}SiO_2$-$3CaO{\cdot}P_2O_5$ solid solution saturated with MgO are shown in Figures 9 and 10 comparing with the activity of P_2O_5 in the $2CaO{\cdot}SiO_2$-$3CaO{\cdot}P_2O_5$ solid solution saturated with CaO.[21] Both the activity and activity coefficient of P_2O_5 increased with the increase of the $3CaO{\cdot}P_2O_5$ content in the solid solution. The activity

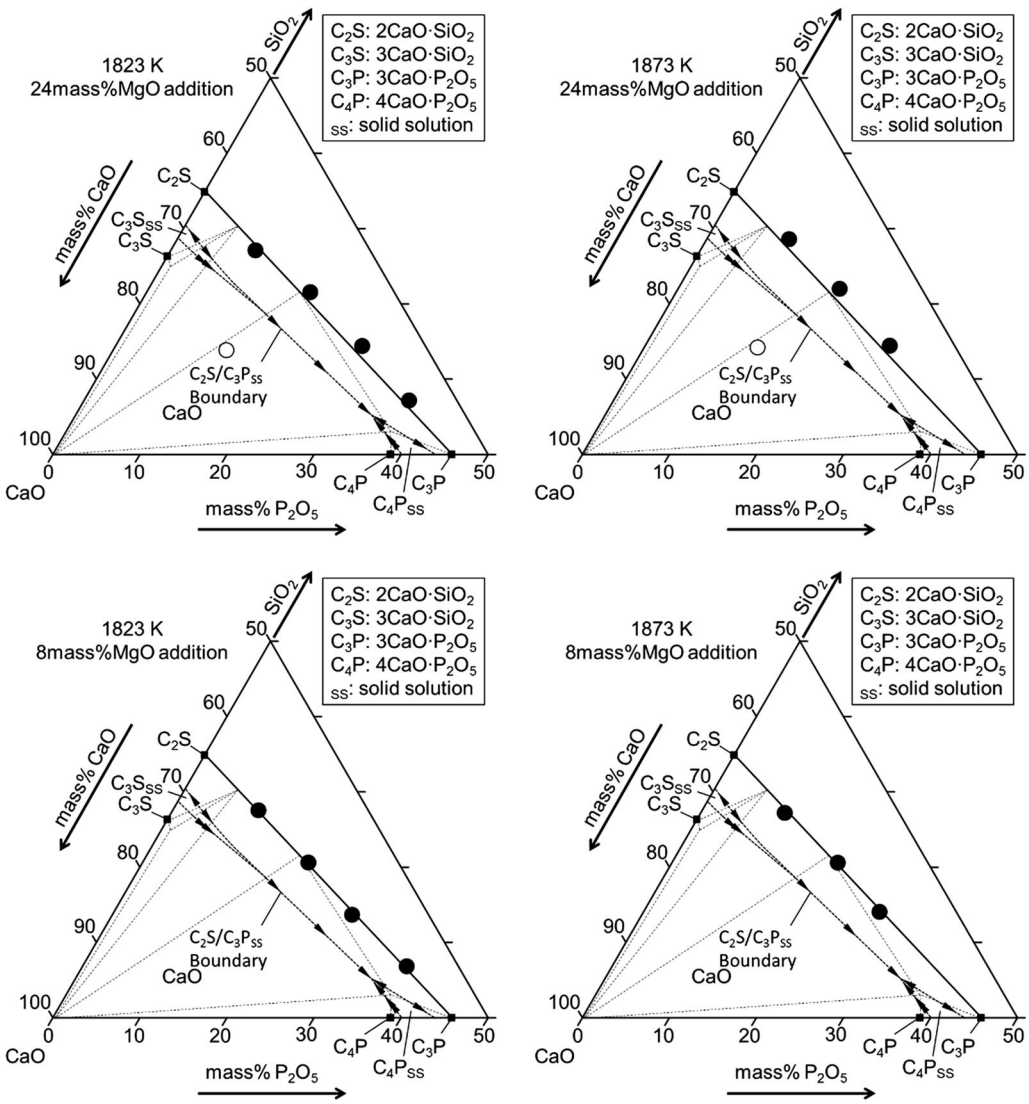

Fig. 4—Projection of the equilibrium composition of oxide specimen onto the $CaO-SiO_2-P_2O_5$ ternary system. The compositions of specimens containing both MgO and CaO phases detected by XRD at equilibrium were marked as open circles.

and activity coefficient at 1873 K (1600 °C) were larger than those at 1823 K (1550 °C) comparing at the same composition of the solid solution. In addition, the activity of P_2O_5 in the $2CaO·SiO_2$-$3CaO·P_2O_5$ solid solution saturated with MgO marked by solid circles and squares was larger than that saturated with CaO marked by open circles and squares in Figures 9 and 10. Furthermore, the activity of P_2O_5 in the $2CaO·SiO_2$-$3CaO·P_2O_5$ solid solution saturated with both CaO and MgO marked by solid triangles was larger than that saturated with CaO and smaller than that saturated with MgO.

The compositions of the $2CaO·SiO_2$-$3CaO·P_2O_5$ solid solution saturated with MgO are projected onto the $CaO-MgO-SiO_2$ and $CaO-MgO-P_2O_5$ systems in Figures 11 and 12. Since the activity of P_2O_5 in the $2CaO·SiO_2$-$3CaO·P_2O_5$ solid solution saturated with MgO increased with the increase of the $3CaO·P_2O_5$ content in the solid solution, the compositions at 1823 and 1873 K (1550 and 1600 °C) cannot locate at the three-phase equilibrium region as shown in Figure 12 with the phase relationship at 1273 K (1000 °C), while experimental results were located in the region. It was because that temperature of the phase diagram in Figure 12 was lower than the present experimental temperature and oxide specimens contained a certain amount of SiO_2. Moreover, not only $2CaO·SiO_2$ and $2MgO·SiO_2$ but also $3CaO·P_2O_5$ and $3MgO·P_2O_5$ could form a solid solution as shown in Figures 11 and 12. Since the phase relationship for the $CaO-MgO-SiO_2$ and $CaO-MgO-P_2O_5$ systems are unavailable at 1823 and 1873 K (1550 and 1600 °C), it was assumed that the composition range of the $2CaO·SiO_2$-$2MgO·SiO_2$ solid solution and the $3CaO·P_2O_5$-$3MgO·P_2O_5$ solid solution increase with the increase of temperature similar to the $2CaO·SiO_2$-$3CaO·P_2O_5$ solid solution.[5]

Since the activity of P_2O_5 in the $2CaO·SiO_2$-$3CaO·P_2O_5$ solid solution saturated with both CaO

Table III. Content of $3CaO{\cdot}P_2O_5$ in the Solid Solution, Partition Ratio of Phosphorus, Activity Coefficient of FeO, and Activities of P_2O_5 and $3MgO{\cdot}P_2O_5$

No.	$3CaO{\cdot}P_2O_5$ (Mol Percent)	$\frac{(\text{Mass Pct P})}{[\text{Mass Pct P}]}$	γ_{FeO}	$\alpha_{P_2O_5}$	$\alpha_{3MgO{\cdot}P_2O_5}$
1-1	13.0	6.26×10^2	16.4	9.24×10^{-25}	1.85×10^{-11}
1-2	26.7	5.00×10^2	15.1	5.59×10^{-24}	1.12×10^{-10}
1-3	45.5	5.24×10^2	14.6	1.17×10^{-23}	2.35×10^{-10}
1-4	69.1	4.27×10^2	19.8	3.16×10^{-23}	6.34×10^{-10}
2-1	12.2	3.91×10^2	12.2	2.26×10^{-24}	3.10×10^{-11}
2-2	26.4	3.60×10^2	7.76	1.05×10^{-23}	1.44×10^{-10}
2-3	45.6	4.25×10^2	7.66	1.75×10^{-23}	2.39×10^{-10}
3-1	12.6	6.02×10^2	19.2	1.46×10^{-24}	2.93×10^{-11}
3-2	27.6	8.36×10^2	17.8	3.00×10^{-24}	5.93×10^{-11}
3-3	45.4	5.31×10^2	17.7	1.56×10^{-23}	3.13×10^{-10}
3-4	69.3	4.01×10^2	23.9	5.17×10^{-23}	1.04×10^{-9}
4-1	12.7	3.77×10^2	12.7	3.53×10^{-24}	4.83×10^{-11}
4-2	27.8	3.52×10^2	17.2	1.64×10^{-23}	2.24×10^{-10}
4-3	44.6	2.91×10^2	20.9	4.99×10^{-23}	6.84×10^{-10}
5-1	28.2	7.07×10^2	12.9	1.31×10^{-24}	2.64×10^{-11}
5-2	28.0	3.00×10^2	8.21	7.22×10^{-24}	9.89×10^{-11}

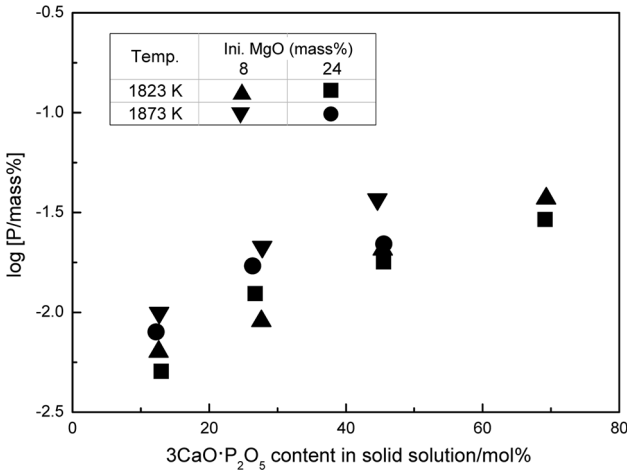

Fig. 5—Content of P in molten iron at equilibrium.

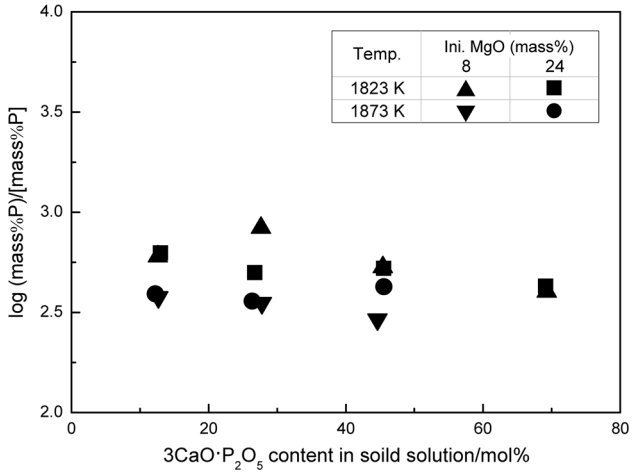

Fig. 6—Phosphorus partition ratio between the $2CaO{\cdot}SiO_2$-$3CaO{\cdot}P_2O_5$ solid solution mixed with MgO and molten iron at equilibrium.

and MgO was smaller than that saturated with MgO, it is considered that the reaction between the solid solution and MgO does not produce a pure CaO phase in the current condition. Therefore, the final composition of the mixture of $2CaO{\cdot}SiO_2$-$3CaO{\cdot}P_2O_5$ solid solution and MgO was the mixture of the $2(Ca,Mg)O{\cdot}SiO_2$-$3(Ca,Mg)O{\cdot}P_2O_5$ solid solution and MgO.

D. *Activity of $3MgO{\cdot}P_2O_5$ in the $2CaO{\cdot}SiO_2$-$3CaO{\cdot}P_2O_5$ Solid Solution Saturated with MgO*

Since the $2CaO{\cdot}SiO_2$-$3CaO{\cdot}P_2O_5$ solid solution was saturated with MgO, the activity of MgO was unity, and thus, the activity of $3MgO{\cdot}P_2O_5$ relative to pure liquid $3MgO{\cdot}P_2O_5$ was calculated from the activity of P_2O_5 by using Eqs. [6] and [7] as shown in Figure 13 as a function of the $3CaO{\cdot}P_2O_5$ content in the solid solution. The activity of $3MgO{\cdot}P_2O_5$ increased with the increase of the $3CaO{\cdot}P_2O_5$ content in the solid solution. The effect of temperature on the activity of $3MgO{\cdot}P_2O_5$ was not clearly observed:

$$3MgO(s) + P_2(g) + 5/2O_2(g) = 3MgO{\cdot}P_2O_5(l),$$

$$\Delta G_6^\circ = -1872000 + 435.1T \text{ J/mol}^{[32]}, \qquad [6]$$

$$P_2(g) + 5/2O_2(g) = P_2O_5(l),$$

$$\Delta G_7^\circ = -1655480 + 571.0T \text{ J/mol}^{[24]}. \quad [7]$$

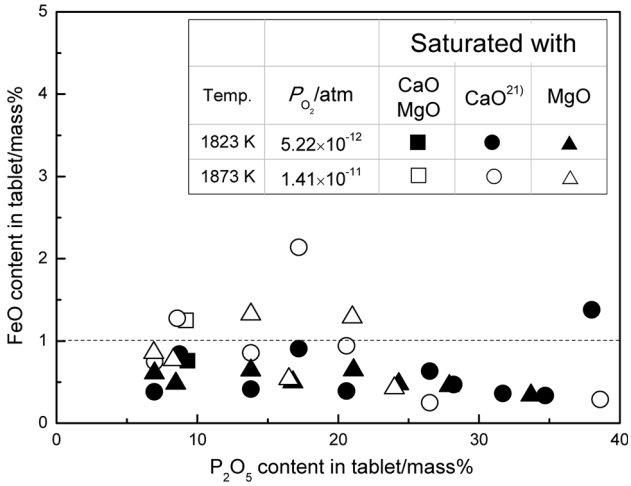

Fig. 7—Content of FeO in the oxide specimen at equilibrium.

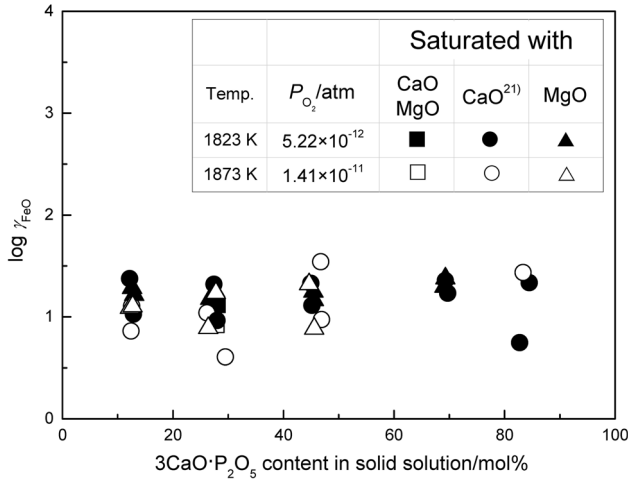

Fig. 8—Activity coefficient of FeO relative to liquid FeO in the solid solution saturated with MgO or CaO at equilibrium.

Table IV. Interaction Coefficients of Solutes in Molten Iron

		j		
e_i^j		P	C	O
i	P	0.054[26]	0.126[27]	0.13[28]
	C	0.051[27]	0.243[25]	−0.32[25]
	O	0.07[28]	−0.421[25]	−0.17[29]

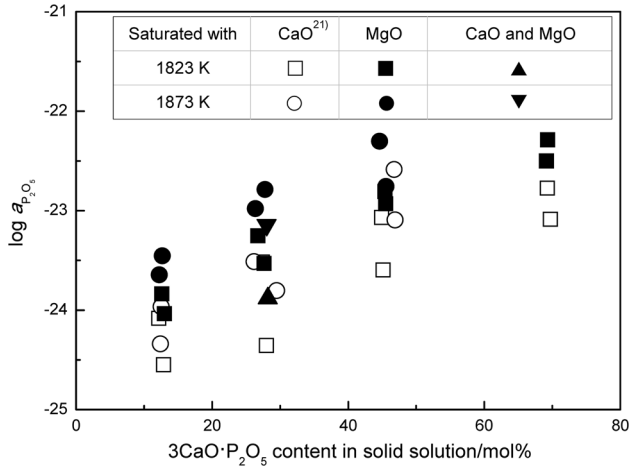

Fig. 9—Activity of P_2O_5 relative to hypothetical pure liquid P_2O_5 in the solid solution.

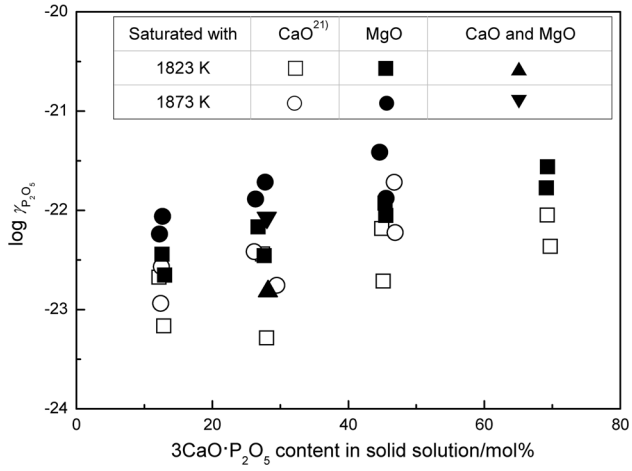

Fig. 10—Activity coefficient of P_2O_5 relative to hypothetical pure liquid P_2O_5 in the solid solution.

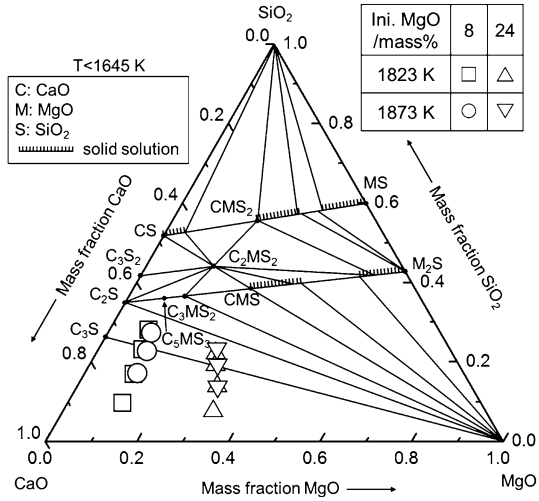

Fig. 11—Projection of the compositions of the $2CaO{\cdot}SiO_2$-$3CaO{\cdot}P_2O_5$ solid solution saturated with MgO at equilibrium on the CaO-MgO-SiO_2 system.[30]

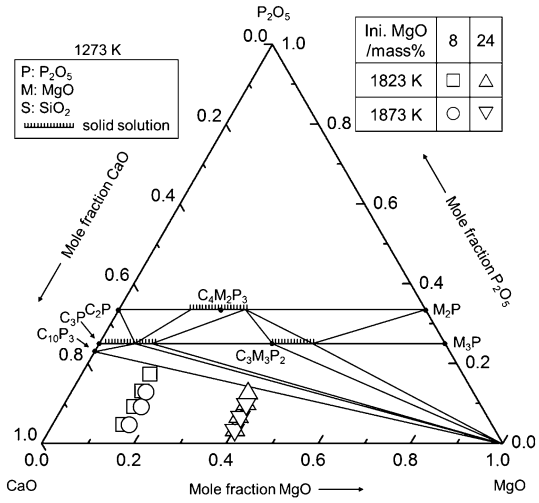

Fig. 12—Projection of the compositions of the $2CaO{\cdot}SiO_2$-$3CaO{\cdot}P_2O_5$ solid solution saturated with MgO at equilibrium on the CaO-MgO-P_2O_5 system.[31]

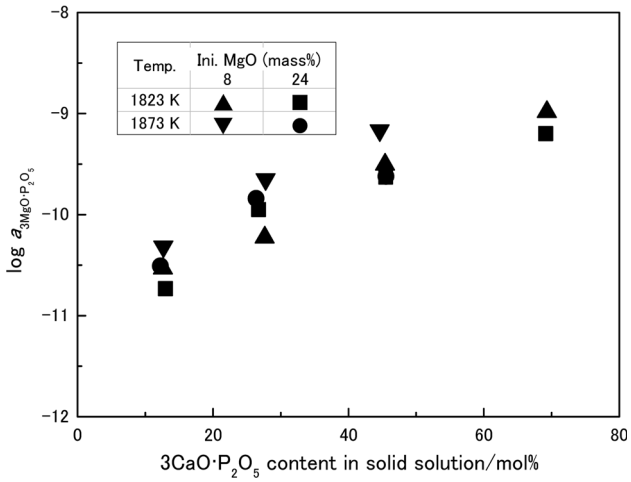

Fig. 13—Activity of $3MgO{\cdot}P_2O_5$ in the $2CaO{\cdot}SiO_2$-$3CaO{\cdot}P_2O_5$ solid solution saturated with MgO.

IV. CONCLUSIONS

By applying the chemical equilibration method, the equilibrium between the $2CaO{\cdot}SiO_2$-$3CaO{\cdot}P_2O_5$ solid solution saturated with MgO and molten iron was observed at 1823 K (1550 °C) with the oxygen partial pressure of 5.22×10^{-12} atm and at 1873 K (1600 °C) with the oxygen partial pressure of 1.41×10^{-11} atm. The activity of P_2O_5 relative to the hypothetical pure liquid P_2O_5 in the $2CaO{\cdot}SiO_2$-$3CaO{\cdot}P_2O_5$ solid solution saturated with MgO increased with the increase of the $3CaO{\cdot}P_2O_5$ content in the solid solution. The activity of P_2O_5 in the solid solution saturated with MgO at 1873 K (1600 °C) was larger than that at 1823 K (1550 °C). In addition, the activity of P_2O_5 in the $2CaO{\cdot}SiO_2$-$3CaO{\cdot}P_2O_5$ solid solution saturated with MgO was larger than that saturated with CaO. The $2CaO{\cdot}SiO_2$-$3CaO{\cdot}P_2O_5$ solid solution mixed with MgO was not saturated with CaO, but the components of the solid solution saturated with MgO were considered to be the mixture of the $2(Ca,Mg)O{\cdot}SiO_2$-$3(Ca,Mg)O{\cdot}P_2O_5$ solid solution and MgO. Moreover, the activity of $3MgO{\cdot}P_2O_5$ in the $2CaO{\cdot}SiO_2$-$3CaO{\cdot}P_2O_5$ solid solution saturated with MgO also increased with the increase of the $3CaO{\cdot}P_2O_5$ content in the solid solution.

REFERENCES

1. R. Viswanathan: *Metall. Trans.*, 1971, vol. 2, pp. 809–15.
2. R. Inoue and H. Suito: *ISIJ Int.*, 2006, vol. 46, pp. 174–79.
3. H. Suito and R. Inoue: *ISIJ Int.*, 2006, vol. 46, pp. 180–87.
4. R. Inoue and H. Suito: *ISIJ Int.*, 2006, vol. 46, pp. 188–94.
5. W. Fix, H. Heymann, and R.S. Heinke: *J. Am. Ceram. Soc.*, 1969, vol. 52, pp. 346–47.
6. F. Pahlevani, S. Kitamura, H. Shibata, and N. Maruoka: *ISIJ Int.*, 2010, vol. 50, pp. 822–29.
7. K. Shimauchi, S. Kitamura, and H. Shibata: *ISIJ Int.*, 2009, vol. 49, pp. 505–11.
8. K. Ito, M. Yanagisawa, and N. Sano: *Tetsu-to-Hagané*, 1982, vol. 68, pp. 342–44.
9. S. Kitamura, S. Saito, K. Utagawa, H. Shibata, and D.G.C. Robertson: *ISIJ Int.*, 2009, vol. 49, pp. 1838–44.
10. T. Hamano, S. Fukagai, and F. Tsukihashi: *ISIJ Int.*, 2006, vol. 46, pp. 490–95.
11. S. Fukagai, T. Hamano, and F. Tsukihashi: *ISIJ Int.*, 2007, vol. 47, pp. 187–89.
12. X. Yang, H. Matsuura, and F. Tsukihashi: *ISIJ Int.*, 2009, vol. 49, pp. 1298–307.
13. X. Yang, H. Matsuura, and F. Tsukihashi: *Tetsu-to-Hagané*, 2009, vol. 95, pp. 268–74.
14. X. Yang, H. Matsuura, and F. Tsukihashi: *ISIJ Int.*, 2010, vol. 50, pp. 702–11.
15. X. Yang, H. Matsuura, and F. Tsukihashi: *Mater. Trans.*, 2010, vol. 51, pp. 1094–101.
16. X. Gao, H. Matsuura, I. Sohn, W. Wang, D.J. Min, and F. Tsukihashi: *Metall. Mater. Trans. B*, 2012, vol. 43B, pp. 694–702.
17. X. Gao, H. Matsuura, I. Sohn, W. Wang, D.J. Min, and F. Tsukihashi: *Mater. Trans.*, 2013, vol. 54, pp. 544–52.
18. X. Gao, H. Matsuura, M. Miyata, and F. Tsukihashi: *ISIJ Int.*, 2013, vol. 53, pp. 1381–85.
19. M. Hasegawa, Y. Kashiwaya, and M. Iwase: *High Temp. Mater. Process.*, 2012, vol. 31, pp. 421–30.
20. M. Zhong, H. Matsuura, and F. Tsukihashi: *ISIJ Int.*, 2015, vol. 55, pp. 2283–88.
21. M. Zhong, H. Matsuura, and F. Tsukihashi: *Mater. Trans.*, 2015, vol. 56, pp. 1192–98.
22. W. Gutt: *Nature*, 1963, vol. 197, pp. 142–43.
23. E.T. Turkdogan: *Physical Chemistry of High Temperature Technology*, Academic Press, New York, 1980, p. 7.
24. S. Ban-ya and S. Matoba: *Tetsu-to-Hagané*, 1962, vol. 48, pp. 925–32.
25. E.T. Turkdogan: *ISIJ Int.*, 2000, vol. 40, pp. 964–70.
26. K. Yamada and E. Kato: *Tetsu-to-Hagané*, 1979, vol. 65, pp. 264–72.
27. H.G. Hadrys, M.G. Frohberg, and J.F. Elliott: *Metall. Trans.*, 1970, vol. 1, pp. 1867–74.
28. D. Dutilloy and J. Chipman: *Trans. Metall. Soc. AIME*, 1960, vol. 218, pp. 428–30.
29. H. Sakao and K. Sano: *J. Jpn. Inst. Met.*, 1959, vol. 23, pp. 671–74.
30. Verein Deutscher Eisenhüttenleute (VDEh) ed.: *SLAG ATLAS*, 2nd edn. Verlag Stahleisen GmbH, Düsseldorf, 1995, p. 134.
31. Verein Deutscher Eisenhüttenleute (VDEh) ed.: *SLAG ATLAS*, 2nd edn. Verlag Stahleisen GmbH, Düsseldorf, 1995, p. 133.
32. E.T. Turkdogan: *Physical Chemistry of High Temperature Technology*, Academic Press, New York, 1980, p. 14.